OPEN ACCESS
IOP Publishing
Journal of Physics A: Mathematical and Theoretical
J. Phys. A: Math. Theor. **57** (2024) 025201 (11pp)
https://doi.org/10.1088/1751-8121/ad10f2

Time-independent, paraxial and time-dependent Madelung trajectories near zeros

Michael Berry

H H Wills Physics Laboratory, Tyndall Avenue, Bristol BS8 1TL, United Kingdom

E-mail: asymptotico@bristol.ac.uk

Received 24 August 2023; revised 2 October 2023
Accepted for publication 29 November 2023
Published 27 December 2023

Abstract

The Madelung trajectories associated with a wavefunction are the integral curves (streamlines) of its phase gradient, interpretable in terms of the local velocity (momentum) vector field. The pattern of trajectories provides an immediately visualisable representation of the wave. The patterns can be completely different when the same wave equation describes different physical contexts. For the time-independent Schrödinger or Helmholtz equation, trajectories circulate around the phase singularities (zeros) of the wavefunction; and in the paraxially approximate wave, streamlines spiral slowly in or out of the zeros as well as circulating. But if the paraxial wave equation is reinterpreted as the time-dependent Schrödinger equation, its Madelung trajectories do not circulate around the zeros in spacetime: they undulate while avoiding them, except for isolated trajectories that encounter each zero in a cusp singularity. The different local trajectory geometries are illustrated with two examples; a local model explains the spacetime cusps.

Keywords: streamlines, vortices, Pearcey, cusp, quantum velocity

1. Introduction

As is well known, the paraxial approximation to the time-independent Schrödinger equation in d-dimensional space, with propagation coordinate y, is mathematically identical to the time-dependent Schrödinger equation in $d-1$ dimensional space, with y replaced by time t [1]. My aim here is to point out a curious geometrical difference between the two cases, reflecting the

fact that they describe different physics. The difference concerns the geometry of trajectories in the Madelung–Bohm representation of wavefunctions [2–5], currently enjoying renewed interest [6–14].

In this representation, a complex scalar wavefunction ψ is expressed in polar form, as the product of a real modulus and a complex exponential phase factor, and the phase gradient of ψ is expressed as a vector field representing a local velocity determining Madelung trajectories. The velocity field is related by continuity to a density given by the square modulus of the wavefunction. The pattern of trajectories provides a vivid picture of the wave. Therefore it is important to understand its geometry, especially near the singularities of the pattern, which are the zeros (phase singularities) of the wavefunction.

It will be explained that there are two patterns of Madelung trajectories, depending on whether a given ψ is regarded as the paraxial approximation to a wave in space, and therefore time-independent, or as a wave in spacetime, and therefore time-dependent. The feature pointed out here is that these patterns are completely different. The differences are most striking for trajectories close to zeros (phase singlularities) of ψ. For waves in space, the trajectories circulate around the zeros, which are therefore also called wave vortices [15–20]. But for waves in spacetime, where propagation is always forward in time, this circulation around zeros cannot occur; instead, trajectories form an unanticipated pattern: they avoid each zero by undulating past it, except for one trajectory that possesses a cusp point there.

Section 2 summarises the underlying theory, and section 3 gives two illustrative examples. In the first (section 3.1), ψ contains two vortices, in a model for which the paraxial approximation is exact; an exactly solvable local model explains the spacetime cusp. Section 3.2 describes a more complicated and physically important wave with a rich pattern of zeros [21], namely the 'diffraction catastrophe' [22] decorating a cusped caustic in the paths of classical mechanics or the rays of geometrical optics.

The wavefunctions in the two examples are not square-integrable. This is irrelevant to the phenomenon identified here, which concerns the local geometry of trajectories near zeros. By transverse modulation, e.g. Gaussian, such waves can be made to represent monochromatic beams of travelling particles with finite energy flux.

An aspect not explored in detail here is the quantum force ∇Q, where Q is the quantum potential [2, 5, 23], proportional to the Laplacian of the modulus of ψ. This force determines how the Madelung trajectories deviate from the classical paths or geometrical rays driven by Newton's equation; often the deviations are undulatory [5, 24] (as envisaged by Isaac Newton himself [25, 26]). The zeros of the quantum potential separate regions where ψ is superoscillatory from regions where it is not [27]; in some cases, the zeros are related to geometrical caustics [28, 29].

For quantum waves, the Madelung–Bohm formalism has often been discussed in connection with interpretations; I am agnostic on such matters and will not consider them here.

2. Madelung trajectories in space and in time

The geometrical phenomenon to be identified is general: it applies to waves in the presence of varying potentials or refractive indices. But for simplicity it will suffice to consider waves ψ propagating freely, i.e. with no external forces, in two-dimensional space. They are governed by the Helmholtz equation, equivalent to the nonrelativistic time-independent Schrödinger equation. With eigenvalue k^2, this equation, and the polar form of ψ, are

$$\nabla^2\psi\left(\boldsymbol{r}\right)+k^2\psi\left(\boldsymbol{r}\right)=0,\ \psi\left(\boldsymbol{r}\right)=\rho\left(\boldsymbol{r}\right)\exp\left(ikS\left(\boldsymbol{r}\right)\right),\ \boldsymbol{r}=\{x,y\}\,. \tag{2.1}$$

In classical mechanics, this corresponds to trajectories generated by the Hamiltonian

$$H_{cl} = \boldsymbol{p}\cdot\boldsymbol{p}, \tag{2.2}$$

so the classical velocity corresponding to momentum $\boldsymbol{p}$ (we ignore mass factors) is

$$\boldsymbol{u}_{cl}(t) = d_t\boldsymbol{r}_{cl}(t) = 2\boldsymbol{p}(t). \tag{2.3}$$

In the Madelung picture [2], the local quantum velocity is proportional to the phase gradient:

$$\boldsymbol{u}(\boldsymbol{r}) = d_t\boldsymbol{r} = 2\nabla S(\boldsymbol{r}) = \frac{2}{k}\mathrm{Im}\frac{\nabla\psi(\boldsymbol{r})}{\psi(\boldsymbol{r})},\ (\boldsymbol{r}=\boldsymbol{r}(t)). \tag{2.4}$$

The phase gradient is a central aspect of wave physics: it appears naturally in at least five different contexts additional to the Madelung picture [30], for example as the local expectation value of momentum as well as velocity and as the weak value of momentum with position postselected. The trajectories $\boldsymbol{r}(t)$, with which we are concerned here, are the streamlines (integral curves) of the velocity field $\boldsymbol{u}(\boldsymbol{r})$.

In the Madelung procedure, the polar representation is substituted into the Helmholtz equation in (2.1) and the real and imaginary parts are separated. This gives the time-independent continuity equation for the current, involving the density ρ^2 :

$$\nabla\cdot\left(\rho^2\boldsymbol{u}\right) = 0, \tag{2.5}$$

and the trajectories also satisfy the Madelung counterpart of Newton's equation for the acceleration:

$$d_{tt}\boldsymbol{r} = d_t\boldsymbol{u}(\boldsymbol{r}) = \boldsymbol{u}(\boldsymbol{r})\cdot\nabla\boldsymbol{u}(\boldsymbol{r}) = \frac{1}{2}\nabla\left(\boldsymbol{u}(\boldsymbol{r})^2\right) = -\nabla Q(\boldsymbol{r}),\ (\boldsymbol{r}=\boldsymbol{r}(t)). \tag{2.6}$$

The quantum potential Q is

$$Q(\boldsymbol{r}) = -\frac{2\nabla^2\rho(\boldsymbol{r})}{k^2\rho(\boldsymbol{r})}. \tag{2.7}$$

The unfamiliar factor 2 results from the absence of the factor $1/2$ in the Hamiltonian (2.2).

If there is a dominant propagation direction y, it is convenient to separate the corresponding exponential factor, and write

$$\psi(\boldsymbol{r}) = \exp(iky)f(\boldsymbol{r}). \tag{2.8}$$

Then, if $f(\boldsymbol{r})$ depends only slowly on y, it satisfies, approximately, the paraxial wave equation:

$$f(\boldsymbol{r}) \approx \psi_p(x,y):\ 2ik\partial_y\psi_p(x,y) = -\partial_{xx}\psi_p(x,y). \tag{2.9}$$

This is a good approximation if all momentum vectors in the Fourier transform of the wave make angles $\theta \ll \pi/2$ with the propagation (y) direction. Then, paraxial Madelung trajectories are similar to those of the Helmholtz equation, apart from an important difference, to be described in section 3.2. If the approximation is exact, as in the case considered in section 3.1, then of course the paraxial Madelung trajectories are identical with those of the Helmholtz equation.

Now replace the coordinate y in (2.9) by time t, and rewrite the paraxial equation:

$$ik\partial_t\psi_p(x,t) = -\frac{1}{2}\partial_{xx}\psi_p(x,t). \tag{2.10}$$

This is the time-dependent nonrelativistic Schrödinger equation for propagation in one space dimension x, with k replaced by 1/Planck's constant, corresponding to the classical Hamiltonian

$$H_{p,cl} = \frac{1}{2}p_x^2. \tag{2.11}$$

After writing this wave in its polar form,

$$\psi_p(x,t) = \rho_p(x,t)\exp(ikS_p(x,t)), \tag{2.12}$$

the Madelung velocity, now directed along x, is

$$u_p(x,t) = d_t x = \partial_x S_p(x,t) = \mathrm{Im}\frac{\partial_x\psi_p(x,t)}{k\psi_p(x,t)},\ (x = x(t)). \tag{2.13}$$

Because the velocity is time-dependent, the trajectory in the x,t plane, i.e. in spacetime, is determined by solving this first-order (and usually nonlinear) differential equation for $x = x(t)$. These x,t trajectories will be contrasted with the Helmholtz or paraxial trajectories in space, i.e. in the x,y plane, determined by (2.4).

For (2.10) the continuity equation is time-dependent:

$$\partial_x\left(\rho_p^2 u_p\right) = -\partial_t\rho_p^2, \tag{2.14}$$

and the Newton equation for the acceleration is

$$\begin{aligned} d_{tt}x = d_t u_p(x,t) &= \partial_t u_p(x,t) + \frac{1}{2}\partial_x\left(u_p(x,t)^2\right) \\ &= -\partial_x Q_p(x,t), \qquad (x = x(t)), \end{aligned} \tag{2.15}$$

with quantum potential

$$Q_p(x,t) = -\frac{\partial_{xx}\rho_p(x,t)}{2k^2\rho_p(x,t)}. \tag{2.16}$$

The reason for not considering either of the quantum potentials (2.7) or (2.16) in detail in the following is redundancy: among the solutions of the Newton equations (2.6) and (2.15) are not only the Madelung trajectories, satisfying the first-order equations (2.4) and (2.13), but infinitely many other evolutions that are not part of the Madelung–Bohm representation of waves. Alternatively stated, general solutions of Newton's equation correspond to specifying the initial position and velocity, but in the Madelung representation the velocity is linked to the position and cannot be specified independently.

In what follows, it will suffice to set $k = 1$, equivalent to measuring position r or coordinate x in units of wavelength/2π.

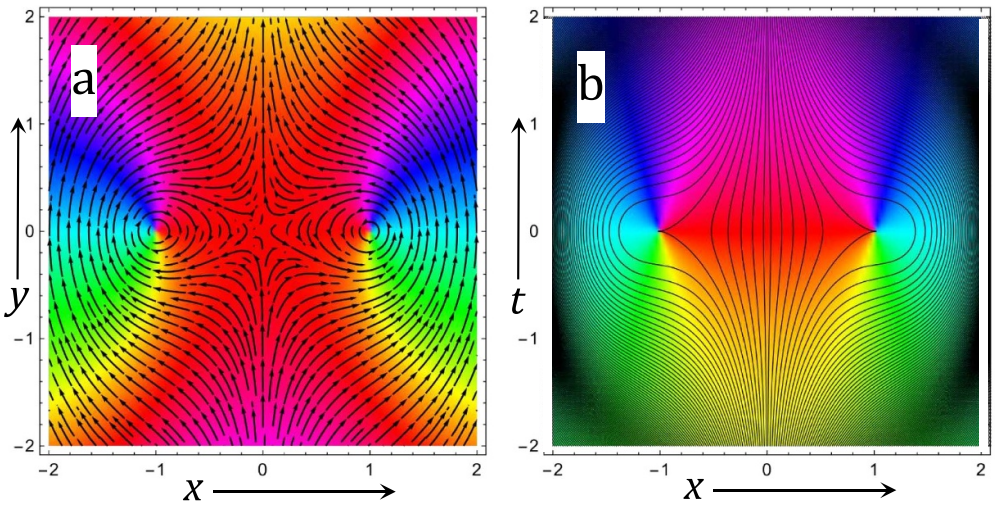

Figure 1. Two-vortex wave. (a) Curves with arrows, Madelung trajectories for solution $\psi(\boldsymbol{r})$ (equation (3.1)) of the Helmholtz equation, superimposed on $\arg\psi(\boldsymbol{r})$, colour-coded by hue. (b) Madelung trajectories for solution $\psi_p(x,t)$ (equation (3.3)) of time-dependent Schrödinger equation, superimposed on $\arg\psi_p(x,t)$ (arrows are unnecessary on these trajectories because they all flow to positive t).

3. Illustrative examples

3.1. Two-vortex model

Among the exact solutions of the Helmholtz equation (2.1) (with $k=1$) are some that are also exact solutions of the paraxial equation (2.9). In terms of the decomposition (2.8), these include waves where $f(\boldsymbol{r})$ is any linear combination of $1, x$ and x^2+iy [31]. We choose the combination

$$\psi(x,y) = \exp(iy)\left(x^2-1+iy\right), \tag{3.1}$$

possessing zeros (phase singularities) at $\{x=\pm1,\ y=0\}$. The Madelung velocity field (2.4) is easily calculated to be

$$\boldsymbol{u}(\boldsymbol{r}) = \left\{\frac{-4xy}{(x^2-1)^2+y^2}, 2+\frac{2\left(x^2-1\right)}{(x^2-1)^2+y^2}\right\}. \tag{3.2}$$

(The term 2 in u_y corresponds to the plane-wave factor $\exp(iy)$).

Figure 1(a) shows the Madelung trajectories (streamlines) of this velocity field, superimposed on the phase field (colour-coded by hue, so the streamlines are orthogonal to the contours of constant hue). Most of the trajectories flow from $y=-\infty$ to $y=+\infty$, but there are two separate families, circulating negatively around the vortex at $x=-1$ and positively around the vortex at $x=+1$.

Figure 1(b) shows the spacetime trajectories of the time-dependent wave

$$\psi_p(x,t) = x^2-1+it, \tag{3.3}$$

superimposed on the corresponding phase field (where the colours look different because in ψ_p the factor $\exp(iy)$ is absent). The trajectories are the solutions $x(t)$ of (cf (2.13)),

$$d_t x = u_p(x,t) = -\frac{2xt}{\left((x^2-1)^2+t^2\right)}, \tag{3.4}$$

with initial conditions $x(-2) = x_0$. It is clear that the trajectories of $\psi_p(x,t)$ are completely different from the streamlines of $\psi(x,y)$, even though the wavefunctions are identical (the factor $\exp(iy)$, is immaterial because it does not shift the zeros and so does not affect the difference in the pattern of trajectories). The trajectories of $\psi_p(x,t)$ bypass each phase singularity instead of circulating round it, except for one trajectory with a cusp point at the singularity.

The cusp can be understood in terms of the simplest local model of a singularity. With coordinates centred on the singularity, this is

$$\psi(x,t) = x + it. \tag{3.5}$$

Its Madelung trajectories $x(t)$ satisfy

$$d_t x = -\frac{t}{x^2+t^2}. \tag{3.6}$$

The solutions of this differential equation are the contours in spacetime of the function

$$c(x,t) = \exp(2x)\left(1+2t^2+2x\ (x-1)\right) \tag{3.7}$$

(Figure 2). Near the vortex, the contour $c(x,t) = 1$ has the form

$$t^2 = -\frac{2}{3}x^3 + \frac{1}{3}x^4 - \frac{2}{15}x^5 + \cdots, \tag{3.8}$$

whose leading term is the cusp. The cusp appears on the side of the spacetime vortex where the x velocity u_p is directed toward the vortex when approaching it in the positive t direction.

Corresponding to the two different patterns of Madelung trajectories are two different quantum potentials. From (3.6), the potential for $\psi(x,y)$ is

$$Q(\boldsymbol{r}) = \frac{2\left(1+5x^4-2x^6+2y^2-2x^2\left(2+3y^2\right)\right)}{\left((x^2-1)^2+y^2\right)^2}. \tag{3.9}$$

And from (2.16) the potential for $\psi_p(x,t)$ is

$$Q_p(x,t) = \frac{4\left(t^2\left(1-3x^2\right)-\left(x^2-1\right)^3\right)}{\left((x^2-1)^2+t^2\right)^2}. \tag{3.10}$$

3.2. Diffraction near a cusped caustic

Cusped caustics in geometrical optics are familiar in reflections inside coffee-cups. These cusps, and the diffraction fine detail that decorates them, can be seen by people wearing glasses on rainy nights, in the distorted several-cusped images of distant lights seen through water-drop 'lenses' on the lenses [32, 33]. And for quantum material particles (e.g. electrons), diffraction

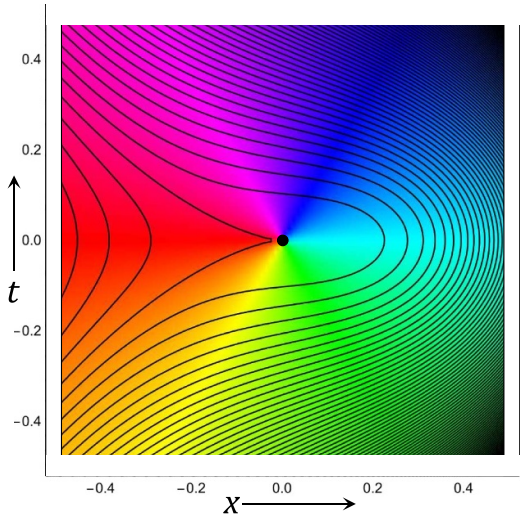

Figure 2. Madelung trajectories (2.8) of the time-dependent wave (3.5) with a single spacetime vortex, superimposed on the phase, showing the cusped trajectory at the phase singularity.

fine detail decorates cusped caustics in the patterns of families of classical paths underlying stationary or time-dependent waves.

The diffraction is described by the Pearcey function [21, 34, 35]. This is an exact solution of the time-dependent Schrödinger equation (2.10) (with $k=1$, though k can easily be reinstated by scaling), so it is convenient to begin by writing the Pearcey function in the variables x,t:

$$\psi_p(x,t) = P(x,t) = \int_{-\infty}^{\infty} \mathrm{d}s \exp\left(i\left(s^4 - ts^2 + xs\right)\right). \tag{3.11}$$

Numerical evaluation (including the required derivatives) is easy after symmetry-reducing the contour to positive s and then rotating it by $+\pi/8$ in the complex s plane.

Figure 3(a) shows a density plot of the modulus $|P(x,t)|$, with the geometrical cusp superimposed. Figure 3(b) shows the time-dependent Madelung trajectories $x(t)$, obtained by numerical solution of the differential equation (2.13), superimposed on the phase $\arg P(x,t)$. The trajectories avoid all the phase singularities, as in the simpler examples in figures 1(b) and 2; and the displayed trajectories include some with cusps near the zeros. (Of course these cusped trajectories, representing fine diffraction detail, must be distinguished from the cusps in the underlying large-scale family of geometrical rays.)

In the spatial plane $\{x,y\}$, $\psi(x,y) = \exp(iy)P(x,y)$ is an exact paraxial solution and an approximate solution of the Helmholtz equation. Figure 3(c) shows the corresponding Madelung trajectories of $\psi(x,y)$. These display the expected circulation around the phase singularities. But there is a difference from the two-vortex case in figure 1(a): the trajectories are not closed. Instead, they spiral into or out of each vortex: the phase singularities are attractors or repellers. Figure 3(d) illustrates this by magnifying the lower rightmost vortex in figure 3(a).

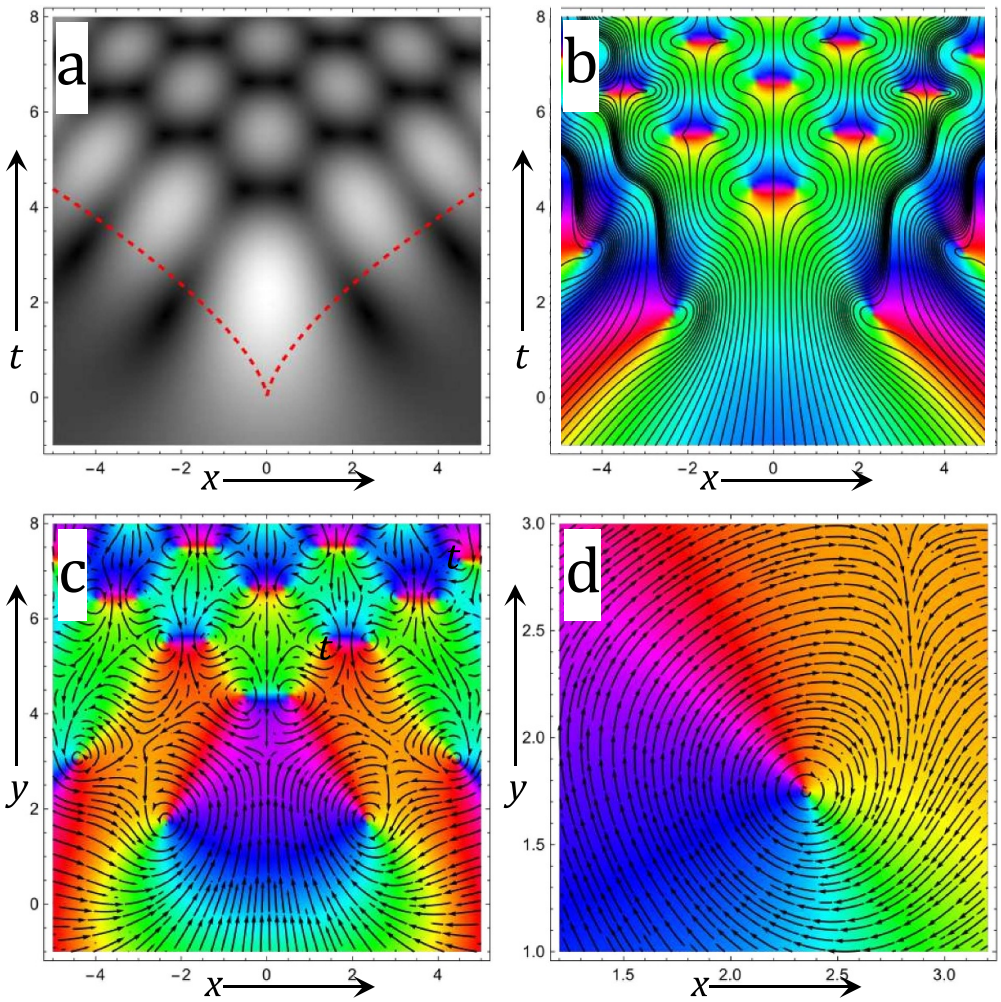

Figure 3. (a) Modulus $|P(x,t)|$ of the Pearcey function (3.11), with the geometrical cusp superimposed; (b) Madelung trajectories in spacetime, superimposed on $\arg P(x,t)$; (c) Madelung trajectories in space, superimposed on $\arg\left(P(x,y)\exp(iy)\right)$; (d) magnification of the lower right vortex, showing the trajectories spiralling as well as circulating.

The spiralling is understood [36]. It is a consequence of $\psi(x,y)$ being an approximate, rather than an exact, solution of the Helmholtz equation. The current $\mathrm{Im}\,\psi^*\nabla\psi$ is not divergenceless as in (2.5), so although the Madelung trajectories are the orthogonal trajectories of the constant-phase contours, they are not themselves contours of a stream function. The spiralling is extremely slow: for small distance r from a phase singularity, the distance between successive windings is $\mathcal{O}\left(r^3\right)$ [36]. In observations, it would be hard to distinguish the spiralling windings from circles.

4. Concluding remarks

It is unsurprising, and certainly not paradoxical, that the same mathematics can arise in different physical contexts. But it is slightly unintuitive, and worth noting, in cases where the contexts are closely related but their manifestations are very different. This is the case for the two manifestations reported here, concerning the local geometries of patterns of Madelung trajectories near zeros; these can be very different for the same wavefunction, when interpreted as a solution of the paraxial equation in space or as the time-dependent Schrödinger equation in spacetime.

Common to optical and quantum waves is the fact that their associated velocity fields are also momentum fields [30]. Therefore they must have dynamical effects; for example, the local momentum vector can exert forces on small particles. This has been explored in the case of stationary optical fields, which can interact with quantum particles, imparting momentum kicks that are especially strong near zeros [37] (though of course the kicks are rare because the wave intensity is small). Analogous forces must also occur for time-dependent quantum fields, and would reflect the different trajectory patterns identified here; this deserves further study.

Here I have illustrated the different Madelung trajectories in the simplest nontrivial situation, where space and spacetime are two-dimensional. In general, the zeros are codimension 2, for example lines when $d = 3$. For three space dimensions, the Madelung trajectories spiral along the singular lines; see [38] for simple optical examples (where the Madelung trajectories are curves tangent to the Poynting vector). For $d = 3$ with two space dimensions and one time dimension, preliminary exploration supports the expectation that the Madelung trajectories behave similarly to the case of $d = 2$ spacetime: most trajectories bypass the singular line, and some are pinched at cusps there. This and other generalisations deserve further study.

Data availability statement

No new data were created or analysed in this study.

Acknowledgments

I thank Professor Gilberto Silva-Ortigoza of Benemérita Universidad Autónoma de Puebla, Mexico, for related correspondence. The paper was written during a visit generously hosted by the International Institute of Physics, Natal, Brazil. This research was supported by an Emeritus Fellowship from the Leverhulme Trust.

ORCID iD

Michael Berry https://orcid.org/0000-0001-7921-2468

References

[1] Marte M A M and Stenholm S 1997 Paraxial light and atom optics: the optical Schrödinger equation and beyond *Phys. Rev.* A **56** 2940–53
[2] Madelung E 1927 Quantentheorie in hydrodynamische form *Z. Phys.* **40** 322–6
[3] Bohm D 1952 A suggested interpretation of the quantum theory in terms of "hidden" variables. I *Phys. Rev.* **85** 166–79

[4] Bohm D 1952 A suggested interpretation of the quantum theory in terms of "hidden" variables. II *Phys. Rev.* **85** 180–93
[5] Takabayasi T 1953 Remarks on the formulation of quantum mechanics with classical pictures and on relation between linear scalar fields and hydrodynamical fields *Prog. Theor. Phys. Japan* **9** 187–222
[6] Heifetz E and Cohen E 2015 Toward a thermo-hydrodynamic like description of Schrödinger equation via the Madelung formulation and fisher information *Found. Phys.* **45** 1514–25
[7] Heifetz E, Tsekov R, Cohen E and Nussinov Z 2016 On entropy production in the Madelung fluid and the role of Bohm's potential in classical diffusion *Found. Phys.* **46** 815–24
[8] Heifetz E and Cohen E 2020 Madelung transformation of the quantum bouncer problem *EPL* **130** 10002
[9] Foskett M S and Tronci C 2023 Holonomy and vortex structures in quantum hydrodynamics, in 'Hamiltonian systems: dynamics, analysis, applications' *Math. Sci. Res. Inst. Pub.* **72** 101–42
[10] Reddiger M 2017 The Madelung picture as a foundation of geometric quantum theory *Found. Phys.* **47** 1317–67
[11] Reddiger M and Poirier B 2023 Towards a mathematical theory of the Madelung equations: Takabayasi's quantization condition, quantum quasi-irrotationality, weak formulations, and the Wallstrom phenomenon *J. Phys. A: Math. Theor.* **56** 193001
[12] Gay-Balmaz F and Tronci C 2020 Madelung transform and probability densities in hybrid quantum-classical dynamics *Nonlinearity* **33** 5383–424
[13] Heifetz E, Guha A and Maas L 2023 de Broglie normal modes in the Madelung fluid *Found. Phys.* **53** 35
[14] Shushi T 2023 Classicality of single quantum particles in curved spacetime through the hydrodynamical reformulation of quantum mechanics *J. Phys. A: Math. Theor.* **56** 365301
[15] Riess J 1970 Nodal structure of Schroedinger wave functions and its physical significance *Ann. Phys.* **57** 301–21
[16] Riess J 1970 Nodal structure, nodal flux fields, and flux quantization in stationary quantum states *Phys. Rev.* D **2** 647–53
[17] Riess J 1987 Quantised vortex motion through rings in quantum mechanics *J. Phys. A: Math. Theor.* **20** 5179–88
[18] Nye J F and Berry M V 1974 Dislocations in wave trains *Proc. R. Soc.* A **336** 165–90
[19] Soskin M S and Vasnetsov M V 2001 Singular optics *Progress in Optics* vol **42** (Elsevier) pp 219–76
[20] Gbur G J 2017 *Singular Optics* (CRC Press)
[21] Berry M V, Nye J F and Wright F J 1979 The elliptic umbilic diffraction catastrophe *Phil. Trans. R. Soc. A* **291** 453–84
[22] Berry M V and Upstill C 1980 Catastrophe optics: morphologies of caustics and their diffraction patterns *Prog. Opt.* **18** 257–346
[23] Holland P 1993 *The Quantum Theory of Motion: An Account of the de Broglie Bohm Causal Interpretation of Quantum Mechanics* (Cambridge University Press)
[24] Berry M V 2009 Optical currents *J. Opt. A: Pure Appl. Opt.* **11** 094001
[25] Berry M V 1997 'Slippery as an eel', review of 'The fire within the eye', by David Park *Phys. World* **10** 41–42
[26] Berry M V 2017 In praise of Whig history, published as approaches to studying our history *Phys. Today* **70** 11–12
[27] Berry M V 2020 Superoscillations and the quantum potential *Eur. J. Phys.* **42** 015401
[28] Espíndola-Ramos E, Silva-Ortigoza G, Sosa-Sánchez C T, Julián-Mácias I, Gonzalez-Juárez A, Cabrera-Rosas O D J and Silva-Ortigoza R 2021 Classical characterization of quantum waves: comparison between the caustic and the zeros of the Madelung-Bohm potential *J. Opt. Soc. Am.* **38** 303–12
[29] Silva-Ortigoza G and Ortiz-Flores J 2023 Properties of the Airy beam by means of the quantum potential approach *Phys. Scr.* **98** 085106
[30] Berry M V 2013 Five momenta *Eur. J. Phys.* **44** 1337–48
[31] Berry M V 1998 Wave dislocations in nonparaxial Gaussian beams *J. Mod. Opt.* **45** 1845–58
[32] Minnaert M 1954 *The Nature of Light and Colour in the Open Air* (Dover)
[33] Berry M V 1976 Waves and Thom's theorem *Adv. Phys.* **25** 1–26
[34] Pearcey T 1946 The structure of an electromagnetic field in the neighbourhood of a cusp of a caustic *Phil. Mag.* **37** 311–7

[35] DLMF 2010 *NIST Handbook of Mathematical Functions* (Cambridge University Press) (available at: http://dlmf.nist.gov)
[36] Berry M V 2005 Phase vortex spirals *J. Phys. A: Math. Theor.* **38** L745–51
[37] Barnett S M and Berry M V 2013 Superweak momentum transfer near optical vortices *J. Opt.* **15** 125701
[38] Berry M V and McDonald K T 2008 Exact and geometrical-optics energy trajectories in twisted beams *J. Opt. A: Pure Appl. Opt.* **10** 035005